Mid-infrared second-order susceptibility of α-quartz and its application to visible-infrared surface sum-frequency spectroscopy

Dennis K. Hore, Mathew Y. Hamamoto, and Geraldine L. Richmond[a)]
Department of Chemistry, University of Oregon, Eugene, Oregon 97403

(Received 10 June 2004; accepted 7 October 2004)

We provide the first account of the second-order susceptibility of quartz down to 10 μm (1000 cm^{-1}) and show how this data may be used along with the sum-frequency response of an amorphous gold surface to elucidate the nonlinear susceptibility of any material in the mid-infrared region. Crystalline quartz is an established material for use in second-harmonic and sum-frequency generation studies of new systems, on account of its well-characterized linear and nonlinear optical properties. Previous knowledge of its nonlinear susceptibility has been limited to its transparent region, wavelengths shorter than about 3 μm. Longer wavelength $\chi^{(2)}$ values for quartz are particularly important for techniques such as vibrational sum-frequency spectroscopy which are expanding into the mid-IR with the increasing availability of widely tunable infrared laser sources. © *2004 American Institute of Physics.* [DOI: 10.1063/1.1826055]

I. INTRODUCTION

Visible-infrared sum-frequency generation spectroscopy is a technique which is ideally-suited to the study of surfaces and buried interfaces.[1–7] Since it is a second-order nonlinear optical method, it inherits its interface specificity from the fact that $\chi^{(2)}$, the second-order susceptibility, is zero in the bulk of centrosymmetric materials (under the electric dipole approximation) but is nonzero at the interface due to the symmetry breaking which occurs there. In contrast with the more established technique of second-harmonic generation, sum-frequency generation using a tunable infrared beam provides information on local vibrational modes, giving it excellent chemical sensitivity.

Crystalline α-quartz has been extensively used as a reference material for second-harmonic and sum-frequency studies for two purposes. First, it may be used to determine the phase of the sum-frequency field by generating an additional sum-frequency signal that interferes with the one from the sample in a homodyne detection scheme.[8–10] Second, the signal generated from quartz may be used to quantify the unknown nonlinear response from new samples.[11] In the first application, it is necessary to work in a wavelength region for which the quartz is transparent since transmission through the quartz is required. Since quartz absorbs light below 3000 cm^{-1} and has many strong bands below 1300 cm^{-1}, it is unsuitable for such an application. In the second application, however, a reflection geometry is often used, making transparency no longer a constraint. As reliable mid-IR laser sources become available, there is growing interest in extending visible-infrared sum-frequency spectroscopy further into the mid-IR. We use our sum-frequency setup to measure the response of quartz in this absorptive region, and thereby determine the dispersion of $\chi^{(2)}$ over these infrared wavelengths.

In addition to calibrating the sum-frequency response of a new material, there is another utility for knowing the nonlinear susceptibility of quartz in the mid-infrared. For wavelengths longer than about 3 μm there are no efficient polarizers which are transparent enough (with a transmittance greater than 70%) for use in controlling the infrared beam polarization. To circumvent this problem, many systems make use of periscopes that change the polarization of the infrared beam by reflection. Since a separate periscope must be installed for *s* or *p* polarization, it is necessary to realign the visible and infrared pump beams to the sample surface, leading to potential differences in spatial and temporal overlap. In addition, it is difficult to adjust both periscopes to have exactly the same path length, resulting in small but significant differences in focusing of the infrared beam at the sample. Both issues may be addressed by comparing the sum-frequency response of the sample with that of a reference compound. For the case of samples with no in-plane ordering (such as liquid surfaces) an amorphous gold sample may be used as a reference. Ordered samples, however, may be investigated with polarization combinations (such as *sss*) that do not provide a sum-frequency response from an amorphous surface. We show that quartz, once the value of $\chi^{(2)}$ is known, and gold together provide an ideal reference combination for quantitatively comparing the signal obtained from different polarization schemes.

The discussion of these topics is presented in three stages. First it is shown that the sum-frequency response from an amorphous gold surface may be used to correct the shape of the quartz spectrum. This is followed by a discussion of how the sum-frequency response from quartz as a function of wavelength and azimuth may be used to determine the dispersion of $\chi^{(2)}$ in the mid-infrared region of interest, from 1000–3050 cm^{-1}. Finally an example is provided of how the measured $\chi^{(2)}$ for quartz is used to determine the nonlinear susceptibility of an ordered polystyrene surface.

[a)]Author to whom correspondence should be addressed. Electronic mail: richmond@uoregon.edu

II. EXPERIMENT

Details of our surface sum-frequency generation experiment may be found in previous publications.[12,13] In brief, we use a regeneratively amplified Ti:sapphire oscillator to produce 1.7 W of 800 nm light with a 2 ps pulse width and a 1 kHz repetition rate. A quarter of the power of this beam is split off for use as the visible pump beam; the other 75% is used to generate an infrared beam which is tunable from 1000–3050 cm^{-1}. This is accomplished by optical parametric generation/amplification in six β-barium borate crystals followed by difference frequency generation in a single silver gallium sulfide crystal. Critical angle tuning of these crystals is controlled by a computer so that the infrared wavelengths may be scanned in a stepwise manner during the experiment. The visible (up to 100 μJ/pulse) and tunable infrared (1–4 μJ/pulse) beams approach the sample surface at 46° and 61°, respectively, from the surface normal. The precise angle of the reflected sum-frequency beam is governed by a phase-matching criterion, and so is dependent on the visible and IR beam angles and frequencies. The detector, a CCD camera, is set to a nominal angle of 50°. The polarization of the two incident beams and that of the detected sum-frequency beam may be selected as either s or p.

III. BASELINE CORRECTION WITH AN AMORPHOUS GOLD SAMPLE

Raw sum-frequency spectra need to be corrected for several experimental artifacts before any quantitative analysis. Regardless of the experimental setup, one of these issues is the variation in IR energy with wavelength, which is a tuning characteristic of the crystals used for parametric generation of the IR frequencies. In nanosecond systems, this may be accomplished simply by measuring the IR energy as a function of wavelength, and dividing the sum-frequency data by this IR spectrum. For picosecond experiments such as ours, this situation is not as simple, since variation in spatial and temporal overlap of the beams as the crystals are tuned must also be taken into account. Details of these issues are given in Ref. 13; in brief, the measured response from a baseline material such as amorphous gold may be used for this purpose. A suitable baseline material will have a large value of $\chi^{(2)}$ in the region of interest, yet any variation in $\chi^{(2)}$ through this wavelength region should be featureless. In such a case, observed spectral features may be attributed to variation in IR energy, spatial, and temporal overlap, and may therefore be used to correct the response of the sample as will be illustrated below.

Ideally, there should also be negligible dispersion of $\chi^{(2)}$ throughout the region of interest (1000–3050 cm^{-1} for this study). While gold gives a strong sum-frequency response, owing to its large second-order susceptibility, its $\chi^{(2)}$ is not entirely free of dispersion through these wavelengths. We neglect the dispersion of $\chi^{(2)}$ for gold in this study, and justify this by a combination of our own experimental findings and theoretical reports in the literature. There are no direct experimental accounts of the variation of $\chi^{(2)}$ with wavelength in the infrared region for gold, but there are a few calculations of this phenomenon.[14–16] The results vary

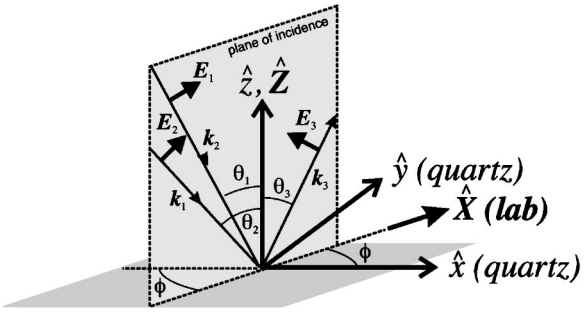

FIG. 1. The plane of all the wave vectors with respect to the crystallographic axes of the quartz sample. The plane of incidence contains the optical (threefold) axis and the surface normal $\hat{z}$. The azimuth of the sample is defined by the angle ϕ that this plane makes with the crystallographic $\hat{x}$ axis.

slightly depending on the level and type of theory employed, but the general trends are the same: there is a small variation in $\chi^{(2)}$ in the near-infrared, from ca. 3000 cm^{-1} to higher frequencies; below 3000 cm^{-1} the dispersion is much less significant. We combine this conclusion with data from previous experimental studies in our group of $\chi^{(2)}$ for dielectric materials (salt solutions and neat D_2O) which show no vibrational resonances from 2800–3800 cm^{-1}, yet have a significant nonresonant response throughout that region.[17,18] In these cases, the raw data showed considerable features due to the variation in IR energy and beam overlap while tuning; dividing by the gold response in the same spectral region resulted in a completely flat nonresonant response for $\chi^{(2)}$ [see, for example, Fig. 1(c) in Ref. 18, and Figs. 4–7 in Ref. 17]. Since the linear and nonlinear optical properties of these dielectric materials are significantly different from that of gold, this is a testament to the fact that neglect of the dispersion of $\chi^{(2)}$ for gold is valid, even for frequencies above 3000 cm^{-1}. The trends revealed by the theoretical papers we mentioned show that as one moves to lower frequencies, the dispersion is even smaller.

The reflected sum-frequency intensity from any surface may be determined from

$$I(\overline{\nu}_3) = \frac{10^4 \overline{\nu}_3^2 \sec^2 \theta_3}{8\varepsilon_0 c} |\chi_{\mathrm{eff}}^{(2),s}|^2 I(\overline{\nu}_1) I(\overline{\nu}_2), \tag{1}$$

where $\overline{\nu}_1$ is the frequency of the visible beam (in cm^{-1}), $\overline{\nu}_2$ the tunable infrared beam, and $\overline{\nu}_3 = \overline{\nu}_1 + \overline{\nu}_2$ is the sum frequency; θ_3 is the exit angle of the sum-frequency beam in air (see Fig. 1). The effective nonlinear surface susceptibility $\chi_{\mathrm{eff}}^{(2),s}$ is related to the actual second-order surface susceptibility $\chi^{(2),s}$ by

$$\chi_{\mathrm{eff}}^{(2),s} = [\mathbf{L}(\overline{\nu}_3)\hat{e}_3] \cdot \chi^{(2),s} : [\mathbf{L}(\overline{\nu}_1)\hat{e}_1][\mathbf{L}(\overline{\nu}_2)\hat{e}_2], \tag{2}$$

where $\mathbf{L}$ are the Fresnel tensors and $\hat{e}_i$ are the unit polarization vectors. The Fresnel factors were determined taking the frequency dependence of the dielectric constant for an amorphous gold surface into account. The complex refractive index data required for these calculations was obtained from Ref. 19. For the $C_{\infty v}$ symmetry of an amorphous gold surface and the ssp polarization scheme,

$$\chi_{\mathrm{eff},ssp}^{(2),s} = -L_{yy}(\overline{\nu}_3)\chi_{yyz}^{(2)} L_{yy}(\overline{\nu}_1) L_{zz}(\overline{\nu}_2) \sin\theta_2. \tag{3}$$

The raw gold sum-frequency spectra are first divided by $|L_{yy}(\overline{\nu}_3)L_{yy}(\overline{\nu}_1)L_{zz}(\overline{\nu}_2)\sin\theta_2|^2$ and then scaled to unity at the wave number for which spatial and temporal overlap was achieved. This provides the baseline for all other scans in the same wave number region since the shape here comes from the variation in IR power, spatial and temporal overlap, square of the sum frequency [see numerator in Eq. (1)] and the exit angle of the sum frequency (since this is a function of frequency, from the phase-matching criterion).

IV. SUM-FREQUENCY FROM α-QUARTZ

Since α-quartz gives a sum-frequency response that displays in-plane anisotropy, the quantitative relation between the orientation in the plane (ϕ, the angle between the crystallographic $\hat{x}$ axis and the laboratory frame $\hat{X}$ axis) and the measured signal needs to be determined. For this we need a form of $\chi^{(2)}$ that can be used in Eqs. (1) and (2) For the ppp polarization scheme used for the quartz measurements there are, in general, eight elements of the $\chi^{(2)}$ tensor which are probed. These are the ones with indices xxx, xxz, xzx, xzz, zxx, zxz, zzx, and zzz. When the effective ppp susceptibility for quartz is expanded into its constituent terms, simplification occurs as a result of the symmetry of the crystal. Crystalline quartz has D_3 symmetry and so the form of its second-order susceptibility tensor[20] is

$$\chi^{(2)}=\begin{bmatrix} xxx & \overline{xxx} & 0 & xyz & xzy & 0 & 0 & 0 & 0 \\ 0 & 0 & 0 & 0 & 0 & \overline{xzy} & \overline{xyz} & \overline{xxx} & \overline{xxx} \\ 0 & 0 & 0 & 0 & 0 & 0 & 0 & zxy & \overline{zxy} \end{bmatrix}, \tag{4}$$

where the overbar denotes negative values. Since $\chi^{(2)}_{xxx}$ is more than two orders of magnitude larger than the other tensor elements,[21] it is customary to assume $\chi^{(2)}_{xyz}=\chi^{(2)}_{xzy}=\chi^{(2)}_{zxy}=0$.[11]

We determine how $\chi^{(2)}$ transforms from the local, crystallographic (xyz) frame under rotation through an in-plane angle ϕ into the laboratory (XYZ) frame where the polarization of the beams is defined. This is accomplished by the Euler transformation

$$\chi^{(2)}_{IJK}=\begin{bmatrix} \cos\phi & \sin\phi & 0 \\ -\sin\phi & \cos\phi & 0 \\ 0 & 0 & 1 \end{bmatrix}\chi^{(2)}_{ijk} \tag{5}$$

which results in

$$\chi^{(2)}_{XXX}=\chi^{(2)}_{xxx}\cos 3\phi \tag{6}$$

and all seven other components of $\chi^{(2)}_{IJK}$ that contribute to ppp equal to zero. For the convenience of those working with other polarization schemes, we have worked out this relation for all combinations of s and p polarizations for the three beams; these results are shown in Table I. Although the polarization schemes shown in the first column of Table I probe the elements of $\chi^{(2)}$ which appear in the second column, the ones appearing in parentheses are equal to zero under the transformation. It is interesting to note then, that each polarization scheme probes only one nonzero element of $\chi^{(2)}$ in the laboratory frame.

Substituting the result for the ppp polarization scheme [Eq. (6)] into Eq. (2), gives

$$\chi^{(2)}_{\mathrm{eff},ppp}=-L_{xx}(\overline{\nu}_3)\cos\theta_3[\chi^{(2),s}_{\mathrm{quartz}}\cos 3\phi] \times L_{xx}(\overline{\nu}_1)\cos\theta_1 L_{xx}(\overline{\nu}_2)\cos\theta_2. \tag{7}$$

Experimental anisotropic refractive index data used for the evaluation of the air-quartz Fresnel coefficients L_{ii} was found in Ref. 22.

Sum-frequency spectra were collected by scanning the IR wavelengths twice in a specific tuning interval, averaging the two scans, then rotating the sample about its normal by 10° and scanning again. This was repeated through a 180° rotation. The raw sum-frequency spectra of quartz were first divided by Fresnel-corrected gold spectra, and then by the square of the product of their own Fresnel factors $|L_{xx}(\overline{\nu}_1)L_{xx}(\overline{\nu}_2)L_{xx}(\overline{\nu}_3)|^2$. This removes the influence of the variation in IR energy, spatial and temporal overlap, sum frequency, and frequency dependence of reflection angle on the spectral shape.

The final factor needed to correct the shape of the apparent quartz spectrum is the coherence length, l_c, of the sum-frequency process, the quantity which relates the surface

TABLE I. Considering that the nonlinear susceptibility tensor for quartz is dominated by $\chi^{(2)}_{xxx}$, we summarize the results of the transformations of this element from the frame of the local crystallographic axes to the laboratory frame by rotation about the surface normal through an azimuthal angle ϕ, for all possible polarization schemes. The elements of $\chi^{(2)}$ in the laboratory frame which appear in parentheses are those which are considered for the particular polarization scheme, but have been determined to be equal to zero.

Polarization scheme	Elements of χ^2 probed in laboratory frame	Transformation of $\chi^{(2)}$ from sample into laboratory frame
sss	YYY	$xxx\sin 3\phi$
ssp	YYX, (YYZ)	$-xxx\cos 3\phi$
sps	YXY, (YZY)	$-xxx\cos 3\phi$
spp	YXX, (YXZ,YXZ,YZZ)	$-xxx\sin 3\phi$
pss	XYY, (ZYY)	$-xxx\cos 3\phi$
psp	XYX, (XYZ,ZYX,ZYZ)	$-xxx\sin 3\phi$
pps	XXY, (XZY,XZY,ZZY)	$-xxx\sin 3\phi$
ppp	XXX, (XXZ, XZX, XZZ, ZXX, ZXZ, ZZX, ZZZ)	$xxx\cos 3\phi$

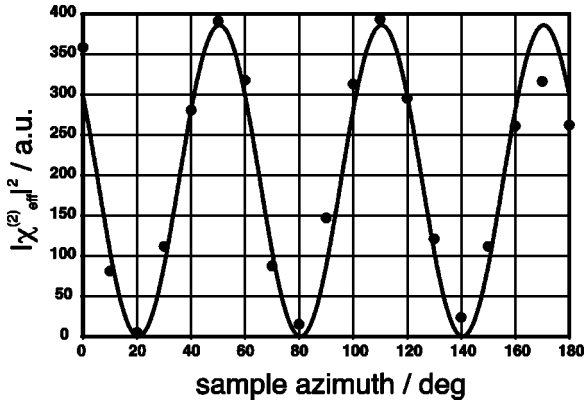

FIG. 2. Sample data, showing the corrected sum-frequency from quartz at 2000 cm^{-1}, compiled from data sets with azimuthal angles ϕ ranging from 0° to 180°. The raw sum frequency from quartz has been divided by the fresnel-corrected and normalized gold scan; then corrected for the quartz fresnel factors and coherence length (also a function of frequency). The only attribute that remains in the signal from quartz is $|\chi^{(2)}_{\mathrm{eff}}|^2$, which may be deduced from the fit. In this data set, it may be seen that ϕ is shifted by $\gamma = 10°$, due to the arbitrary placement of the sample. This appears as an effective shift of 30° since the intensity is proportional to $\cos^2(3\phi - 3\gamma)$.

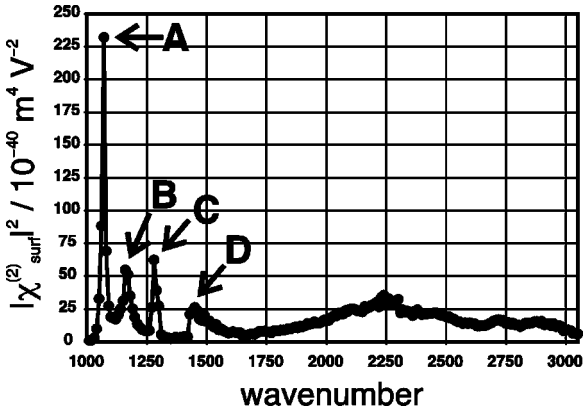

FIG. 3. The final result, after compilation of all data sets, is a plot of the square of the surface nonlinear susceptibility of α-quartz from 1000–3050 cm^{-1}. Peaks (A) at 1082 cm^{-1} and (B) at 1170 cm^{-1} are quartz fundamental modes. Peak (C) at 1280 cm^{-1} is a combination band from lower-energy modes. The band at 1430 cm^{-1} (D) is likely due to a carbonate impurity.

second-order susceptibility to the bulk value as $\chi^{(2),s}_{\mathrm{quartz}} = l_c \chi^{(2),\mathrm{bulk}}_{\mathrm{quartz}}$. This may be obtained from[11]

$$|l_c| = \left| \frac{1}{k_z(\overline{\nu}_1) + k_z(\overline{\nu}_2) + k_z(\overline{\nu}_3)} \right|$$
$$= |200\pi(\overline{\nu}_1\sqrt{n(\overline{\nu}_1)^2 - \sin^2\theta_1} + \overline{\nu}_2\sqrt{n(\overline{\nu}_2)^2 - \sin^2\theta_2} + \overline{\nu}_3\sqrt{n(\overline{\nu}_3)^2 - \sin^2\theta_3})|^{-1}, \quad (8)$$

where $k_z(\overline{\nu})$ is the z component of the wave vector at frequency $\overline{\nu}$ (in wave numbers) travelling in the sample. At our highest IR frequency of 3050 cm^{-1}, $l_c = 35$ nm. After dividing the result in progress by a factor proporitional to $|l_c|^2$, the remaining variation in line shape is due only to the frequency dependence of the bulk nonlinear susceptibility. This treatment was applied to spectra acquired in five overlapping wavelength regions, 1000–1300 cm^{-1}, 1200–2000 cm^{-1}, 1700–2200 cm^{-1}, 1800–3100 cm^{-1}, and 2850–3050 cm^{-1}.

The next step is to examine the data as a function of azimuth rather than wavelength. The azimuthal data for each wavelength was fit to Eq. (7) as $|\chi^{(2),s}_{\mathrm{eff}}|^2 \propto |\chi^{(2),s}_{\mathrm{quartz}} \cos 3\phi|^2 = A\cos^2(3\phi - 3\gamma)$, where γ is the displacement of the crystallographic x axis from the laboratory frame X axis at $\phi = 0$ due to the arbitrary placement of the (unmarked) quartz sample. The value of γ does not affect our result or enter into subsequent calculations, but must be determined to achieve the proper fit. An example is shown in Fig. 2 for data assembled for all azimuthal angles corresponding to $\overline{\nu}_2 = 2000$ cm^{-1}. After fitting the azimuthal data for every wavelength, $|\chi^{(2),s}_{\mathrm{quartz}}|^2$ is determined to within arbitrary units, and the scaling varies for each spectral region. However, the overlapping regions between scans may be used to scale the data consistently over the entire 1000–3050 cm^{-1} range.

The last step to creating a quantitative spectrum of $|\chi^{(2),s}|^2$ for α-quartz is to take the piecewise joined data and determine the constant of proportionality required to set the scale to absolute units for the effective surface susceptibility. Several authors have used a quartz reference for IR wavelengths as long as 3.5 μm (2850 cm^{-1}) (Refs. 11 and 23) since this is still far enough from absorption bands to use the literature value for the bulk nonlinear susceptibility at 1064 nm. This YAG fundamental is the longest wavelength for which $\chi^{(2)}$ has been previously determined. We use the value of the signal proportional to $|\chi^{(2)}|^2$ at our highest frequency, 3050 cm^{-1}, and determine the constant of proportionality required to set that value to $|\chi^{(2)} l_c|^2$ at 1064 nm. There are several determinations of $\chi^{(2)}_{xxx}$ for quartz in the literature, both experimental[24–27] and from calculation;[28,29] we use the value from Ref. 21 of $\chi^{(2)}_{xxx} = 2d_{11} = 0.7$ pm V^{-1}. The surface susceptibility at 3050 cm^{-1} is then used to scale the entire plot, now in MKS units of m^4 V^{-2} as shown in Fig. 3.

There are a number of reports of experimental and computational studies of quartz normal modes.[30–35] The largest mode at 1082 cm^{-1}, labeled as (A) in Fig. 3 and also the peak at 1170 cm^{-1} (B) are the two highest energy quartz normal modes among the eight which are both IR and Raman active.[30] The peak at 1280 cm^{-1} (C) is a combination band from lower-energy modes. The band at 1430 cm^{-1} (D) cannot be assigned to any of the Si–O modes, but is characteristic of α-quartz (absent in IR spectra of fused quartz and other silicate glasses[34]), and may be due to $CaCO_3$ inclusion.[36] This peak, as well as the broad feature from 1750–3000 cm^{-1} may be due to the specific crystal in our investigation. The procedure we outline here is applicable to any material, and may therefore be used to calibrate and subsequently use another quartz sample or different material. The application of this will be illustrated in the following section.

V. USING THE QUARTZ SUSCEPTIBILITY FOR SUM-FREQUENCY STUDIES OF MATERIALS IN THE MID-IR

Having arrived at the second-order susceptibility of quartz in the mid-infrared region down to 1000 cm^{-1}, we present an application for the use of this data in the determi-

nation of the nonlinear susceptibility of a sample with undetermined nonlinear optical properties. Visible-infrared sum-frequency spectra of a well-ordered polystyrene sample were acquired from 1000–1650 cm^{-1} with *ppp* polarization. (The detailed study of ordered polystyrene in this wavelength region will be discussed in a later paper.) As in the case of the quartz spectra, the first step is to remove features that come from the variation in IR energy, spatial, and temporal overlap as the IR frequencies are scanned. This is accomplished by first acquiring an *ssp* sum-frequency spectrum from an amorphous gold surface over the same frequency region. The gold spectum is divided by the square of the product of its fresnel coefficients (as described above) and then scaled to unity at the frequency for which spatial and temporal overlap were achieved (1200 cm^{-1} in this case). After dividing the raw polystyrene data by this scaled, fresnel-corrected gold data, we have the actual sum-frequency response from the polymer, proportional to the square of its effective second-order susceptibility.

The absolute units of $|\chi^{(2),s}_{\text{eff}}|^2$ may be recovered by measuring the sum-frequency response from quartz at a frequency within the region of interest, and preferably where there is a large response from the sample. The IR frequency was therefore set to 1450 cm^{-1} and the sum-frequency response of quartz was measured as a function of azimuthal angle. Since the value for only a single wave number is required, the azimuth was varied from 0° through a full 360° in 10° increments. Equation (7) shows that the maximum sum-frequency response will occur at $\phi=0$ when the quartz x axis is aligned with the laboratory frame X axis (or $\phi=n\pi/3$ due to the six-fold symmetry of the response). Although it should therefore be possible to position the quartz for a measurement of a single one of these maxima, we achieve a much more accurate determination of this value by measuring over several periods and then fitting to $A\cos^2(3\phi-3\gamma)$ as explained in the preceding section.

At 1450 cm^{-1} this fit determined that $A=9200$ counts. Since any value measured in this way is affected by variation in IR energy and spatial and temporal overlap with wavelength, this value should also be adjusted using the Fresnel-corrected and scaled gold spectrum. Overlap of the beams on gold was achieved at 1200 cm^{-1} and the normalized spectrum shows that there is 1.14 times more signal at 1450 cm^{-1} than at 1200 cm^{-1}. The quartz calibration value is therefore corrected to $A'=A/1.14=8070$ counts.

The raw polystyrene data, and therefore the now baseline-corrected polystyrene sum-frequency spectrum, are in units of detector counts. We may relate the observed counts in the corrected polystryene spectrum to the 8070 counts attributed to the effective nonlinear susceptibility of quartz. Figure 3 shows that at 1450 cm^{-1}, $|\chi^{(2)}_{\text{quartz}}|^2=26\times10^{-40}$ $m^4\,V^{-2}$. We first determine the effective susceptibility at this wavelength as

$$\begin{aligned}|\chi^{(2),\text{eff}}_{\text{quartz}}|^2&=|L_{xx}(\overline{\nu}_3)\cos\theta_3 L_{xx}(\overline{\nu}_1)\cos\theta_1 L_{xx}(\overline{\nu}_2)\\&\quad\times\cos\theta_2|^2|\chi^{(2),s}_{\text{quartz}}|^2\\&=(0.008\,718)(26.1\times10^{-40}\ \text{m}^4\,\text{V}^{-2})\\&=2.3\times10^{-41}\ \text{m}^4\,\text{V}^{-2}\end{aligned}\tag{9}$$

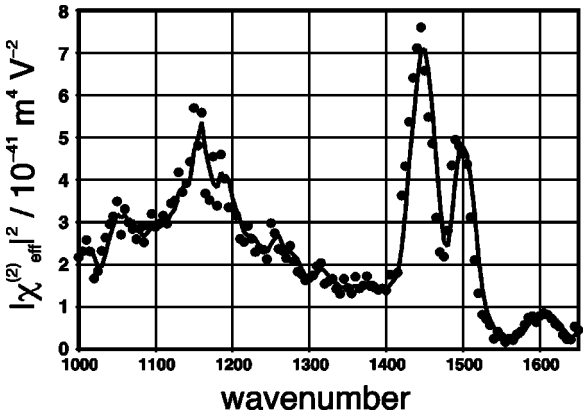

FIG. 4. The square of the effective susceptibility as a function of wave number for an oriented polystyrene sample, acquired with the *ppp* polarization scheme. This was obtained from the raw sum-frequency scan according the method we describe using both gold and quartz. Points are experimental data; the solid line is a guide to the eye, obtained by performing a moving average over five points.

and then determine the appropriate scaling factor for all the wavelengths from

$$|\chi^{(2),\text{eff}}_{\text{sample}}|^2(\overline{\nu}_2)=\text{counts}(\overline{\nu}_2)\frac{2.3\times10^{-41}\ \text{m}^4\,\text{V}^{-2}}{8070\ \text{counts}}.\tag{10}$$

This is applied to the polystyrene spectrum to obtain the final result, shown in Fig. 4. Resonance enhancement of $\chi^{(2)}$ occurs when the infrared frequency $\overline{\nu}_2$ matches the energy of a vibrational transition. Although a more detailed treatment would involve spectral deconvolution, a few characteristic peaks may be observed. These include six C═C ring modes, 1015 cm^{-1} (Varsanyi mode 18a), 1150 cm^{-1} (mode 9b), 1175 cm^{-1} (9a), 1452 cm^{-1} (19b), 1493 cm^{-1} (19a), and 1601 cm^{-1} (8a).[37]

VI. CONCLUSIONS

We have used visible-infrared sum-frequency spectroscopy to measure the dispersion of the second-order susceptibility of α-quartz from 1000–3050 cm^{-1}. This constitutes the first report of this nonlinear optical quantity for quartz for wavelengths this long into the mid-infrared, extending into the lattice bands of the crystal. We have demonstrated a method which uses both gold and quartz responses to arrive at the effective surface susceptibility of uncharacterized surfaces. The application of these findings to the study of polystyrene is demonstrated for its ring modes in the mid-infrared. These results have important implications for future vibrational sum-frequency studies that seek to measure surface vibration modes throughout the infrared spectral region.

ACKNOWLEDGMENTS

The authors thank R. Haydock and E. Raymond for helpful discussions. The authors acknowledge Energy Sciences of the Department of Energy for support of this science and the Office of Naval Research for the instrumentation.

[1] Y. R. Shen, in *Proceedings of the International School of Physics, Ernico Fermi*, edited by T. W. Hansch and M. Inguscio (North-Holland, Amsterdam, 1994), pp. 139–165.
[2] Y. R. Shen, *The Principles of Nonlinear Optics* (Wiley, New York, 1984).
[3] Y. R. Shen, Annu. Rev. Phys. Chem. **40**, 327 (1989).
[4] G. L. Richmond, Chem. Rev. (Washington, D.C.) **102**, 2693 (2002).
[5] G. L. Richmond, Annu. Rev. Phys. Chem. **52**, 357 (2001).
[6] K. B. Eisenthal, Chem. Rev. (Washington, D.C.) **96**, 1343 (1996).
[7] C. T. Williams and D. A. Beattie, Surf. Sci. **500**, 545 (2002).
[8] R. Superfine, J. Y. Huang, and Y. R. Shen, Chem. Phys. Lett. **172**, 303 (1990).
[9] R. Superfine, J. Y. Huang, and Y. R. Shen, Opt. Lett. **15**, 1276 (1990).
[10] R. K. Chang, J. Ducuing, and N. Bloembergen, Phys. Rev. Lett. **15**, 6 (1965).
[11] X. Wei, S.-C. Hong, X. Zhuang, T. Goto, and Y. R. Shen, Phys. Rev. E **62**, 5160 (2000).
[12] D. E. Gragson, B. M. McCarty, G. L. Richmond, and D. S. Alavi, J. Opt. Soc. Am. B **13**, 2075 (1996).
[13] D. K. Hore, J. L. King, F. G. Moore, D. S. Alavi, M. Y. Hamamoto, and G. L. Richmond, Appl. Spectrosc. **58**, 1376 (2004).
[14] W. L. Schaich, Phys. Rev. B **61**, 10478 (2000).
[15] A. Liebsch, Appl. Phys. B: Lasers Opt. **68**, 301 (1999).
[16] A. Liebsch and W. L. Schaich, Phys. Rev. B **40**, 5401 (1989).
[17] E. A. Raymond and G. L. Richmond, J. Phys. Chem. B **108**, 5051 (2004).
[18] E. A. Raymond, T. L. Tarbuck, and G. L. Richmond, J. Phys. Chem. B **106**, 2817 (2002).
[19] D. W. Lynch and W. R. Hunter, in *Handbook of Optical Constants of Solids*, edited by E. D. Palik (Academic, San Diego, 1985), see chapter on comments on the optical constants of metals and an introduction to the data for several metals, pp. 290–295.
[20] P. N. Butcher and D. Cotter, *The Elements of Nonlinear Optics* (Cambridge University Press, New York, 1990).
[21] S. Singh, in *CRC Handbook of Lasers*, edited by R. J. Pressley (Chemical Rubber Co., Cleveland, 1971), Chap. 18, p. 499.
[22] H. R. Philipp, in *Handbook of Optical Constants*, edited by E. D. Palik (Academic, San Diego, 1985), pp. 719–747.
[23] X. Wei, S.-C. Hong, A. I. Lvovsky, H. Held, and Y. R. Shen, J. Phys. Chem. B **104**, 3349 (2000).
[24] I. Shoji, T. Kondo, A. Kitamoto, M. Shirane, and R. Ito, J. Opt. Soc. Am. B **14**, 2268 (1997).
[25] R. C. Miller, Phys. Rev. **131**, 95 (1963).
[26] R. Hellwarth, J. Cherlow, and T.-T. Yang, NBS Spec. Publ. **414**, 207 (1974).
[27] C. Flueraru and C. Grover, Appl. Opt. **42**, 6666 (2003).
[28] Z. H. Levine, Int. J. Quantum Chem. **28**, 411 (1994).
[29] M.-Z. Huang and W. Y. Ching, Ferroelectrics **156**, 105 (1994).
[30] R. A. Murray and J. G. Gualtierii, *Fundamental Lattice Vibrations in Quartz* (Institute of Electrical and Electronics Engineers, Piscataway, NJ, 1989), pp. 477–484.
[31] W. G. Spitzer and D. A. Kleinman, Phys. Rev. **121**, 1324 (1961).
[32] J. W. Foise, *1997 IEEE International Frequency Control Symposium* (Institute of Electrical and Electronics Engineers, Piscataway, NJ, 1997), pp. 527–535.
[33] H. J. Hrostowski and R. H. Kaiser, Phys. Rev. **107**, 966 (1957).
[34] J. R. Ferraro, M. H. Manghnani, and A. Quattrochi, Phys. Chem. Glasses **13**, 116 (1972).
[35] J. D. Hardy and S. Silverman, Phys. Rev. **37**, 176 (1931).
[36] S. Silverman, Phys. Rev. **39**, 72 (1932).
[37] G. Varsanyi, *Assignments for Vibrational Spectra of Seven Hundred Benzene Derivatives* (Halsted, New York, 1974), Vol. 1.